RSC Advances

ROYAL SOCIETY OF CHEMISTRY

www.rsc.org/advances

Study on coating growth characteristics during the electrolytic oxidation of magnesium-lithium alloy by optical emission spectroscopy analysis

Zhongping Yao, Qixing Xia, Han Wei, Dongqi Li, Qiu Sun, Zhaohua Jiang

School of Chemical Engineering and Technology, State Key Laboratory of Urban Water Resource and Environment, Harbin Institute of Technology, Harbin 150001 PR China

Abstract: The aim of this work is to analyze the composition and structure and the growth characteristic of the plasma electrolytic oxidation (PEO) coatings through the optical emission spectroscopy (OES). The PEO coatings were prepared on the magnesium-lithium alloy in the phosphate system at different frequencies. The composition and structure of the coatings were examined by X-ray diffraction (XRD), X-ray photo-electron spectroscopy (XPS) and scanning electron microscopy (SEM) equipped with energy dispersive X-ray (EDX). The discharge sparks of the PEO process were collected by optical emission spectroscopy. The results show that the PEO coating prepared at 50 Hz is composed of crystallized MgO and crystallized $Mg_3(PO_4)_3$ and the coating at 500 Hz is composed of crystallized MgO and amorphous $Mg_3(PO_4)_3$. The coating prepared at 50Hz has a larger roughness than that at 500 Hz, and the sizes of the micro pores on the coating prepared at 50 Hz are much larger than that at 500 Hz whereas the numbers of the micro pores at different frequencies change quite oppositely to the pore sizes. The plasma temperature (T_e) calculated with OES at 50 Hz is about 3100 K higher than that at 500 Hz, which means that more energy generated per cycle was applied to the electrode surface at 50 Hz than 500 Hz, influencing the structure and composition of the coatings consequently. Based on the OES analysis, the growth characteristic of the PEO coatings was proposed to explain the changes of the coating roughness and

the formation mechanism of crystallized or amorphous $Mg_3(PO_4)_3$ at different working frequencies by the T_e and the liquid-cooling effect, which was further proved by the designed experiments changing the electrical parameters of the PEO process. This work also illustrates that the adjustment of the phase composition and structure by the electrical parameters can be well explained by OES. Besides, the corrosion resistance of the MAO coatings was evaluated by the polarizing curves in 3.5 wt.% NaCl solution. The corrosion resistance of the coatings is mainly determined by the thickness and roughness and the coatings prepared under 500 Hz generally present better corrosion resistance than those under 50 Hz.

Keywords: Plasma electrolytic oxidation; Ceramic coatings; Optical emission spectroscopy; Plasma temperature; Magnesium-Lithium alloy

1. Introduction

The plasma electrolytic oxidation (PEO), also known as micro-arc oxidation (MAO) or anodic spark deposition (ASD), is one of the electrochemical coating techniques in the proper electrolytes by plasma discharges on the valve metals (Al, Ti, Mg etc.) and their alloys[1, 2]. The PEO coatings have excellent properties such as anti-abrasion, corrosion resistance and many other functional properties, which present the promising application prospects in the fields of aerospace, biomaterial[3, 4] and catalysis[5, 6] and so on. The PEO process is composed of a series of complex reactions including the migration of ions, dielectric breakdown and formation and dissolution of oxide layer, especially for the spark discharges[7, 8], which have a significant influence on the structure, composition and phase formation of the PEO coatings.

Recently, the optical emission spectroscopy (OES) has been becoming a more and more popular method to study the spark discharges during the PEO process in various electrolytes on aluminum[9-11], tantalum[12], magnesium[9, 13, 14] and titanium[15]. By detecting the feature lines in OES, the plasma temperature (T_e) and electron concentration (N_e) can be calculated[10, 16]. Li Wang[17] examined the OES

in the PEO process on Mg alloys in different electrolytes and the electron temperature of the excited hydrogen was between 6×10^3 and 3×10^4 K by H_β lines. RO Hussein[10] calculated the T_e of PEO reactions on pure Al and the T_e (by Al I lines) increases with the current density enhanced. J Jovović[13, 18] have researched the PEO spectra on Mg, Al and Ta alloys and the spectra were divided into discharging luminescence and discharging strong ionic/atomic emission. Therefore, the OES technique presents a unique advantage over the research of PEO process and mechanism, and much more work is extremely needed to disclose the coating formation mechanisms by this technique, especially the proper combination of OES technique with the traditional analyzing methods.

The change of the phase composition is one important aspect to reveal the PEO process and growth mechanism, which are influenced by the substrate, the electrolytes and the technique parameters[19-21]. As reported, the composition of PEO coatings on Mg alloy in the phosphate-based electrolyte is only crystallized MgO phase with a large amount of amorphous P under the higher working frequencies[22-24]. Quite oppositely, crystallized $Mg_3(PO_4)_2$ phase was detected under the lower working frequencies[14, 24-27]. However, the reason for this change of phase composition is not further well explained in the above references due to their different research targets. In this work, the coatings with different composition were prepared in the phosphate electrolyte on Mg-Li alloys. OES technique was used to obtain the spectra during the PEO process and the growth mechanism was proposed to explain the changes of the phase composition and structure and further proved by the designed experiments changing the electrical parameters of the PEO process.

2. Experimental details

2.1 Preparation of ceramic coatings

Plate specimens of size 40 mm ×40 mm × 2 mm from Mg-Li alloy with a nominal composition of 4% lithium and 96% magnesium in mass fraction. They were mechanically polished with 240, 600, 1000 and 2000 grit SiC sandpaper and cleaned with distilled water before PEO treatment. A homemade single pulse power of 10 kW was used for plasma electrolytic oxidation of sample in

phosphate-based electrolyte composed of hexametaphosphate (4 g/L), sodium polyphosphate (0.8 g/L), sodium hydroxide (4 g/L) and sodium fluoride (1g/L). The cleaned specimens were served as anode in a water-cooled electrochemical bath made of stainless steel which used as cathode. The coating on Mg-Li substrate was prepared at constant current density i of 5 A/dm^2. The PEO treatments were carried out for different times ranged from 300 s to 500 s at 50 Hz and 500 Hz, respectively. The duty ratios of both pulses were both equal to 20%. The temperature of the electrolyte was controlled in 10-20 °C with a cooling water flow. After PEO treatment, the obtained specimens were cleaned with distilled water and dried in air.

2.2 Analysis of Composition and Structure of the PEO coatings

The thickness and roughness of PEO coating were investigated using thickness gauge (CTG-10, Time Company, China) and roughness tester (TR200, Time Group Inc., China). The morphology and element distribution of surface and cross-section were analyzed by field emission scanning electron microscope (FE SEM, FEI, QUANTA-200F, America) equipped with energy dispersive X-ray spectrometer (EDS, Oxford Model 7537, America). D/Max-2400 X-ray diffraction was used to characterize the phase composition. The composition and chemical states of the elements on the PEO coating surface were investigated by X-ray photoelectron spectroscopy (XPS; PHI 5700 ESCA System, Al $K\alpha$, 1486.6eV, America).

2.3 The Optical emission spectroscopy

The Ocean Optics Sensor OES (QE6500, Ocean optics, America) was used to characterize the spectrum within the wavelength range 200-900 nm in the PEO process. The total spectrum was collected per three seconds with integral time 500 ms. The plasma temperature was calculated based on the calculated equation shown in Eq (1)[10, 12], where I (1) and I (2) are relative line intensities of lines of the same species in question, $A_{mn}(i)$ the transition probabilities, m the upper level of the respective lines, $g_m(i)$ the statistical weight of the upper levels, $\lambda_0(i)$ the wavelengths of the line centers in vacuum, $E_m(i)$ are energies of the upper levels of lines and k_BT the thermal energy[28].

$$\frac{I(1)}{I(2)} = \frac{A_{mn}(1)\,g_m(1)\lambda_0(2)}{A_{mn}(2)\,g_m(2)\lambda_0(1)} \exp-\left\{\frac{E_{m(2)} - E_{m(1)}}{k_B T}\right\} \quad \text{Eq (1)}$$

2.4 Evaluation of corrosion resistance

Corrosion resistance of the coatings was evaluated in a conventional three-electrode electrochemical cell (a Pt plate was used as a counter electrode, a calomel electrode as the reference electrode, and the coated sample with the area of 1 cm^2 as the working electrode) through CHI660B electrochemical analyzer (Chenhua, Shanghai, China) in 3.5 wt. % NaCl solution at room temperature. The samples were soaked in NaCl solution for about 60 min to make sure that the open-circuit potential (OCP) of the samples was stabilized before the electrochemical measurement. The Tafel curve was measured from −250 mV to +250 mV of OCP with a sweep rate of 1.0 mV/s.

3. Results and discussion

3.1 Voltage–time curves

The voltage-time curves in the course of PEO process at 50 Hz and 500 Hz are shown in Fig. 1. According to changing trend of voltage-time curves, the entire PEO process is divided into three stages. At the stage A (0-60 s), the frequency almost does not influence the breakdown voltage and the increase rate of the voltage, the dense tiny white sparks emerges on the substrate electrode surface at around 330V. At the stage B (60-540 s), the voltage curve of 50 Hz increases slowly while the voltage of 500 Hz increases at a relatively high rate of 19 V/min. Afterwards, the voltage of both frequencies increases more slowly with the similar growth rate of 3 V/min at the stage C, and the voltage difference between two frequencies was kept at about 70 V at this stage.

3.2 Morphologies and composition of the PEO coatings

The prepared ceramic coatings are white and uniform on the macro scale. Fig. 2 shows that the prepared ceramic coatings have the typical porous morphology. The size of micro pores on the

coating prepared for 300s at 50 Hz is uniform is from 5 μm to 20 μm. Increasing the PEO time to 1200s, the size of pores further increased to 50-100μm. Moreover, the micro cracks emerge on the coating surface. The coatings prepared at 500Hz are much smoother than those at 50Hz. When the PEO time is 1200s, the size of the pores is a little increased while the coating smoothness is reduced. This is consistent with the results of the roughness measurement in SI Fig.1. SI Table 1 shows the coating is composed of a large amount of Mg, O and P and a little Na and F, and the relative content of each element on the surface of the PEO coating is similar for both kinds of coatings.

The cross-sectional morphologies of ceramic coatings are shown in Fig. 3. The thickness increased with the PEO time for the coatings prepared at two frequencies, which is consistent with the results of the thickness measurement in SI Fig. 1. At the short working time (less than 900s), two kinds of coatings have the similar thickness. When the PEO time is beyond 900s, the coatings at 500 Hz are thicker than those at 50 Hz. There are many micro pores and fissures along the coating section images. For the coating prepared for 300s at 50 Hz, some of the micro pores are connected with the inner and penetrated to the substrate. Fig. 4 shows the relative content of the main elements along the cross section of the PEO coatings. The elemental distribution differences are focused on the interface between the substrate and the coating. Otherwise, the relative contents of all the elements are stable along the cross section of the coatings, except for the big falls in the positions with many defects such as pores or cracks within the coating.

Fig. 5 shows the X-ray diffraction patterns of the coatings. The peaks corresponding to $Li_{0.92}Mg_{4.08}$ (pdf: 65-4080) were evidently characterized. Extending the PEO time, the peaks of $Li_{0.92}Mg_{4.08}$ were gradually decreased due to the increase of the coatings thickness. Besides $Li_{0.92}Mg_{4.08}$, the coatings obtained at 50 Hz are composed of crystallized $Mg_3(PO_4)_2$ (pdf: 75-1491) and MgO (pdf: 77-2179). There are no crystallized $Mg_3(PO_4)_2$ peaks detected for the coatings

obtained at 500 Hz. The mound peaks in 2θ range of 20°~ 40° shows that there may be some amorphous compound in the coatings, related to phosphate from the electrolyte.

In order to further investigate the composition of the coatings, the XPS analysis was conducted with the full XPS spectrum shown in SI Fig. 2, which shows that the coating is composed of Mg, P, O, F and Na, the same as the results of EDS analysis. Fig. 6 shows the high-resolution spectra of major elements in the PEO coatings. As shown in Fig. 6 (a, b), the typical Mg 1s spectra is fitted to two kinds of chemical states at peaks 1304.4 eV and 1305.3 eV, which are corresponding to magnesium hydroxide and magnesium phosphate[29], respectively. The typical P 2p spectra shown in Fig. 6 (c, d) can be fitted into two peaks at 133.4 eV and 134.1 eV. The peak at 133.4 eV corresponds to PO_4^{3-}, and another peak at 134.1 eV corresponds to PO_3^- which might come from the electrolytic solution[30, 31]. The typical O 1s spectra shown in Fig. 6 (e, f) can be fitted into three peaks. The fitted peaks for O 1s at 531.4 eV, 532.10 eV and 533.3 eV are corresponding to PO_4^{3-}, MgO and PO_3^-, respectively[29, 31]. According to the XPS analyses, both of the coatings have the similar compositions. Combined with the XRD analyses, it can be proved that the crystallized MgO is formed in both coatings, and the crystallized $Mg_3(PO_4)_2$ is generated in the coatings prepared at 50 Hz while the amorphous $Mg_3(PO_4)_2$ is generated in the coatings prepared at 500 Hz.

3.3 The OES spectra and The OES analysis of the PEO growth process

Fig. 7 shows the emission spectroscopy of PEO process at (a) 50 Hz and (b) 500 Hz. SI Table 2 shows the main spectral lines observed in the spectroscopy with the wavelength[28]. The PEO spectroscopy contains sodium, hydrogen α and β, oxygen (Na, H and O, from the electrolyte), lithium and magnesium (Li and Mg from the substrate). During the entire PEO process, the emission spectra at 500 Hz are obviously stronger than that at 50 Hz. The yellow spark discharge is corresponding to the emission line of Na I (589.0 nm) which is the strongest in the entire spectroscopy.

The typical time variation of different plasma emission intensities during the PEO process at 50

Hz and 500 Hz is shown in Fig. 7 (c) and (d). In the spectra, the intensity of all the typical emission spectra presents the same changing trends as the PEO time. Combined with the results of the voltage-time curves, the emission lines could be rarely detected until 300 seconds and then the intensities of the spectrum increases rapidly. The strength of all emission spectra at 50 Hz continuously increase until 850 s and then slightly decreases afterwards, which means the PEO reaction at 50 Hz become weak after 850 s so that the increasing trend of the prepared coating slows down whereas the emission spectra at 500 Hz first increase until around 400 s and then keep stable at a high strength thereafter with the increasing trend of the prepared coating larger than that at 50 Hz, as shown in SI Fig. 1.

Fig. 8 shows typical time variation of T_e (by Na I lines) and Na (589.0 nm)/Li (670.8 nm) ratios (b) at 50 Hz and 500 Hz. The T_e was calculated to be 8300±830 K to 16000±1600 K at 50 Hz and the T_e was 5200±520 K to 14000±1400 K at 500 Hz, as shown in Fig. 8 (a), the former is about 3100 K higher than the latter, which is related to the duration time per cycle. At 50 Hz, the duration time per cycle is 4 ms, 10 times longer than that (0.4 ms) at 500Hz, which means that more continuous energy from the power source is applied to the electrode surface each cycle. Consequently, severer discharge and larger sparks or micro arcs were observed in the experimental process of 50 Hz, which leads to the increase of the roughness and the pore size on the coating surface, compared with the coating prepared at 500 Hz. This complies with the results from the SEM analysis and the roughness measurement.

The high T_e also is liable for the excitation of Li from the substrate; therefore much more Li joined the plasma discharge process at 50 Hz than at 500 Hz, with the results shown in Fig.8b. However, the contents of Na and Li are much lower than those of O, Mg and P based on the EDS and XPS analysis. Therefore, the main role of Na and Li in the PEO process is to fulfill the electric discharge, which forms the electron current during the PEO process. Their contribution on the coating growth is much smaller than that of element O, Mg and P. This is consistent with the refs[10, 12].

Interestingly, the strength of the spectrum line of H is also much lower, which is different with many other references[10, 17]. This is may be related to element Li from the alloys.

During the PEO process, the formation of the crystallized substances is dependent on the plasma temperature and the quick-cooling effect of the electrolyte. At 50 Hz, the higher T_e makes the micro reaction zone melt sufficiently and the higher duration time with the high energy each cycle weakens the quick-cooling effect of the electrolyte, which provides the enough phase transmission time from the amorphous state to the crystalline. Therefore, the crystallized $Mg_3(PO_4)_3$ is formed in the coating. However, the sizes and the lifetime of spark discharges at 500 Hz are relatively smaller and shorter so that the amorphous state still remains without enough phase transmission time due to the quick-cooling effect. MgO with higher melting point (3073 K) has the much higher formation rate of crystallization nuclei than $Mg_3(PO_4)_3$ during the PEO process, so the crystallized MgO is formed in the coating at both frequencies, as shown in Fig. 9.

Therefore, the formation of the crystallized $Mg_3(PO_4)_3$ is related to the T_e, the duration time per cycle and the liquid-cooling effect, which are determined by the electrical parameters of the PEO process. In order to verify this, the effects of different electrical parameters in the PEO process on the phase composition were investigated, with the results shown in Fig.9. Fig. 9 (a) further shows that the diffraction peaks of $Mg_3(PO_4)_3$ become weaker and weaker with the increase of working frequency and the crystallized $Mg_3(PO_4)_3$ does not appear in the coating prepared at 100 Hz. Fig. 9 (b) presents that the increase of the duty cycle and the current density give rise to the formation of crystallized $Mg_3(PO_4)_3$. Actually, decreasing the working frequency, increasing the duration time per cycle or improving the current density are beneficial for the increase of T_e (confirmed in SI Fig. 4) and the reduction of the liquid-cooling effect, which is liable for the formation of crystallized $Mg_3(PO_4)_2$.

3.4 Corrosion resistance of the coatings

Fig. 10 is the polarizing curves of the MAO coatings and Mg-Li alloy substrate and in 3.5 wt.%

NaCl solution. The fitting values of the corrosion potential (E_{corr}), the corrosion current density (I_{corr}) and the polarization resistance (R_p) are shown in Table 1. By comparison of I_{corr} and R_p, it can be indicated that the corrosion resistance of the MAO coatings is much better than that of the substrate and the MAO coatings prepared under 500 Hz are better than those under 50 Hz.

Combined with the characterization and OES analysis above, it can be concluded that the corrosion resistance of the coatings is not mainly determined by the crystalized or un-crystalized composition of the coatings, but by the coating thickness and roughness. The larger the thickness and the lower the roughness, the better the corrosion resistance is. Under 50 Hz, the coating prepared for 15 min has the best corrosion resistance, which is due to the opposite effects of the thickness and roughness of the coatings. Under 500 Hz, increasing the reaction time, the coating thickness increases greatly whereas the roughness does not improve apparently compared with the thickness; therefore, the corrosion resistance of the coatings is increased with the reaction time gradually under the experimental conditions.

4. Conclusions

(1) The PEO coatings on Mg-Li alloy have typical porous structure. With the increase of the frequency, the pore sizes decrease while the pore numbers increase. The coatings prepared at 50 Hz are composed of crystallized $Mg_3(PO_4)_2$ and MgO, while the coatings at 500Hz are composed of crystallized MgO and amorphous $Mg_3(PO_4)_2$.

(2) The PEO conditions are mainly provided by the Na and Li discharges based on the OES and the plasma temperature of the PEO process at 50 Hz is higher 3100 K than at 500 Hz calculated by Na lines. The electric discharges of Na and Li in the PEO process form the electron current, but do less contribution to the growth of the PEO coating.

(3) Based on the OES analysis, the phase composition of the coatings is related to the plasma temperature and the duration per cycle, which can be adjusted by the electrical parameters.

Decreasing the working frequencies, increasing the duty cycle or the current density is helpful for the formation of crystallized $Mg_3(PO_4)_2$.

(4) The MAO coatings greatly improved the corrosion resistance of the Mg-Li alloy substrate and the corrosion resistance of the MAO coatings prepared under 500 Hz is better than that under 50 Hz. Under 50 Hz the coating prepared for 15 min has the best corrosion resistance. Under 500 Hz the corrosion resistance of the coatings is increased with the reaction time gradually under the experimental conditions.

Acknowledgement

This work was supported by Shanghai Aerospace Science and Technology Innovation Fund Projects (Grant No. SAST201431) and State Key Laboratory of Urban Water Resource and Environment (Harbin Institute of Technology) (No. 2015DX07).

The authors have declared no conflict of interest.

References

1. A. Yerokhin, X. Nie, A. Leyland, A. Matthews and S. Dowey, *Surface and Coatings Technology*, 1999, **122**, 73-93.
2. F. Walsh, C. Low, R. Wood, K. Stevens, J. Archer, A. Poeton and A. Ryder, *Transactions of the IMF*, 2009, **87**, 122-135.
3. M. Montazeri, C. Dehghanian, M. Shokouhfar and A. Baradaran, *Applied Surface Science*, 2011, **257**, 7268-7275.
4. D. Sreekanth and N. Rameshbabu, *Materials Letters*, 2012, **68**, 439-442.
5. K. Kageyama, J.-i. Tamazawa and T. Aida, *Science*, 1999, **285**, 2113-2115.
6. Y. Yoshida, S. Matsui and T. Fujita, *Journal of organometallic chemistry*, 2005, **690**, 4382-4397.
7. A. Yerokhin, L. Snizhko, N. Gurevina, A. Leyland, A. Pilkington and A. Matthews, *Journal of Physics D: Applied Physics*, 2003, **36**, 2110.
8. A. Yerokhin, X. Nie, A. Leyland and A. Matthews, *Surface and Coatings Technology*, 2000, **130**, 195-206.
9. Stojadinovic, S., Vasilic, R., Belca, I., Petkovic, M., Kasalica and B., *Corrosion Science*, 2010, 3258-3265.
10. R. Hussein, X. Nie, D. Northwood, A. Yerokhin and A. Matthews, *Journal of Physics D:*

Applied Physics, 2010, **43**, 105203.

11. M. Sarvan, J. Radic-Peric, B. Kasalica, I. Beica, S. Stojadinovic and M. Perice, *Surface & Coatings Technology*, 2014, **254**, 270-276.
12. S. Stojadinović, N. Tadić and R. Vasilić, *Electrochimica Acta*, 2015, **152**, 323-329.
13. J. Jovović, 2014.
14. J. Liang, P. B. Srinivasan, C. Blawert, M. Störmer and W. Dietzel, *Electrochimica Acta*, 2009, **54**, 3842-3850.
15. R. O. Hussein, X. Nie and D. O. Northwood, *Materials Chemistry and Physics*, 2012, **134**, 484–492.
16. J. Jovović, S. Stojadinović, N. M. Šišović and N. Konjević, *JOURNAL OF QUANTITATIVE SPECTROSCOPY & RADIATIVE TRANSFER*, 2012, **113**, 1928–1937.
17. L. Wang, L. Chen, Z. Yan and W. Fu, *Surface and Coatings Technology*, 2010, **205**, 1651-1658.
18. J. Jovović, S. Stojadinović, N. M. Šišović and N. Konjević, *Surface and Coatings Technology*, 2011, **206**, 24–28.
19. S. Stojadinović, R. Vasilić, M. Petković, I. Belča, B. Kasalica, M. Perić and L. Zeković, *Electrochimica Acta*, 2012, **59**, 354-359.
20. S. Stojadinović, R. Vasilić, M. Petković and L. Zeković, *Surface and Coatings Technology*, 2011, **206**, 575-581.
21. H. Li, V. Rudnev, X. Zheng, T. Yarovaya and R. Song, *Journal of Alloys and Compounds*, 2008, **462**, 99-102.
22. A. Da Forno and M. Bestetti, *Surface and Coatings Technology*, 2010, **205**, 1783-1788.
23. R. Zhang, D. Shan, R. Chen and E. Han, *Materials Chemistry and Physics*, 2008, **107**, 356-363.

24. P. Bala Srinivasan, J. Liang, R. Balajeee, C. Blawert, M. Störmer and W. Dietzel, *Applied Surface Science*, 2010, **256**, 3928-3935.

25. Q. Cai, L. Wang, B. Wei and Q. Liu, *Surface and Coatings Technology*, 2006, **200**, 3727-3733.

26. S. Yagi, A. Sengoku, K. Kubota and E. Matsubara, *Corrosion Science*, 2012, **57**, 74-80.

27. A. M. Kumar, S. H. Kwon, H. C. Jung and K. S. Shin, *Materials Chemistry and Physics*, 2014.

28. J. E. Sansonetti, W. C. Martin and S. Young, *Journal of Physical and Chemical Reference Data*, 2005, **34**, 1559-2260.

29. X. Cui, Q. Li, Y. Li, F. Wang, G. Jin and M. Ding, *Applied Surface Science*, 2008, **255**, 2098-2103.

30. Y. Barbaux, M. Dekiouk, D. Le Maguer, L. Gengembre, D. Huchette and J. Grimblot, *Applied Catalysis A: General*, 1992, **90**, 51-60.

31. H. Zhang, G. Yao, S. Wang, Y. Liu and H. Luo, *Surface and Coatings Technology*, 2008, **202**, 1825-1830.

List of Table captions

Table 1 Fitting results of the polarization curves of the coatings and the Mg-Li alloy substrate

Table 1 Fitting results of the polarization curves of the coatings and the Mg-Li alloy substrate

Samples	Time /min	E_{corr}/V	I_{corr}/A·cm^{-2}	R_p/Ω·cm^2
Mg-Li alloy	0	-1.547	4.54×10^{-4}	87.1
50Hz	5	-1.440	1.84×10^{-5}	1379.8
	10	-1.387	9.36×10^{-6}	2785.8
	15	-1.353	4.80×10^{-6}	5363.5
	20	-1.338	1.44×10^{-5}	1969.7
500 Hz	5	-1.182	2.40×10^{-6}	15656.6
	10	-1.150	1.96×10^{-6}	19168.2
	15	-1.066	2.02×10^{-6}	20122.2
	20	-0.860	1.58×10^{-6}	22522.4

List of figure captions

Fig. 1 Voltage–time responses during PEO processing of Mg-Li alloy at 50 Hz and 500 Hz

Fig. 2 The surface morphologies of the coatings prepared at (a) 300 s, 50 Hz; (b) 1200 s, 50 Hz; (c) 300 s, 500 Hz; (d) 1200 s, 500 Hz

Fig. 3 Cross-sectional SEM images of the ceramic coatings

Fig. 4 The relative content of element distribution on the cross section of the PEO coatings prepared at (a) 50 Hz and (b) 500 Hz

Fig. 5 XRD patterns of the ceramic coating prepared at different times, and the PEO frequency are (a) 50 Hz and (b) 500 Hz

Fig. 6 The high-resolution spectra of major elements in the PEO coatings. (a) Mg 2p, 50 Hz; (b) Mg 2p, 500 Hz; (c) P 2p, 50 Hz; (d) P 2p, 500 Hz; (e) O ls, 50 Hz; (f) O 1s, 500 Hz

Fig. 7 Plasma Spectroscopy of PEO process at (a) 50 Hz and (b) 500 Hz for 900 s and typical time variation of the emission line intensity during the PEO process at 50 Hz (c) and 500 Hz (d)

Fig. 8 Typical time variation of T_e by Na I lines (a) and Na 589.0 nm / Li 670.8 nm ratios (b) at 50 Hz and 500 Hz

Fig. 9 XRD patterns of the PEO coating prepared (a) at different frequencies in duty ratio 20%, 5 A/dm^2 and (b) in different current density and duty ratio at 80 Hz

Fig. 10 Tafel polarization curves of the MAO coatings and Mg-Li alloy substrate. (a) 50 Hz and (b) 500 Hz

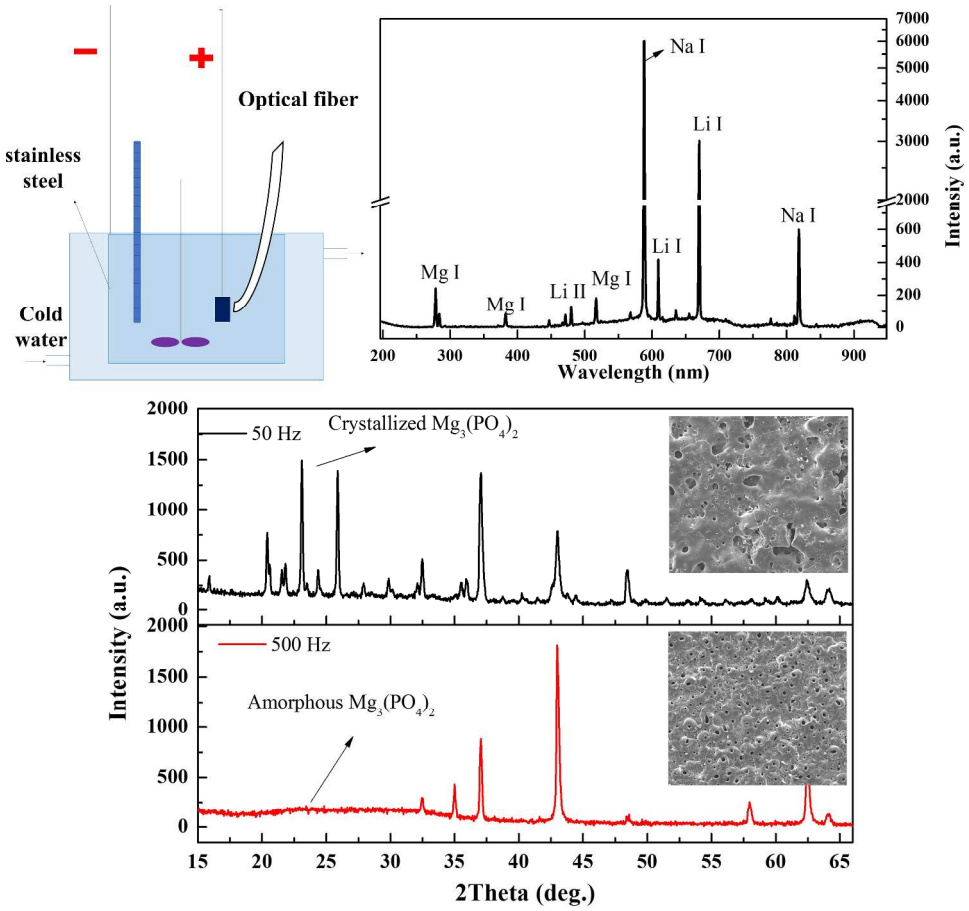

Graphical Absrtact
867x781mm (150 x 150 DPI)

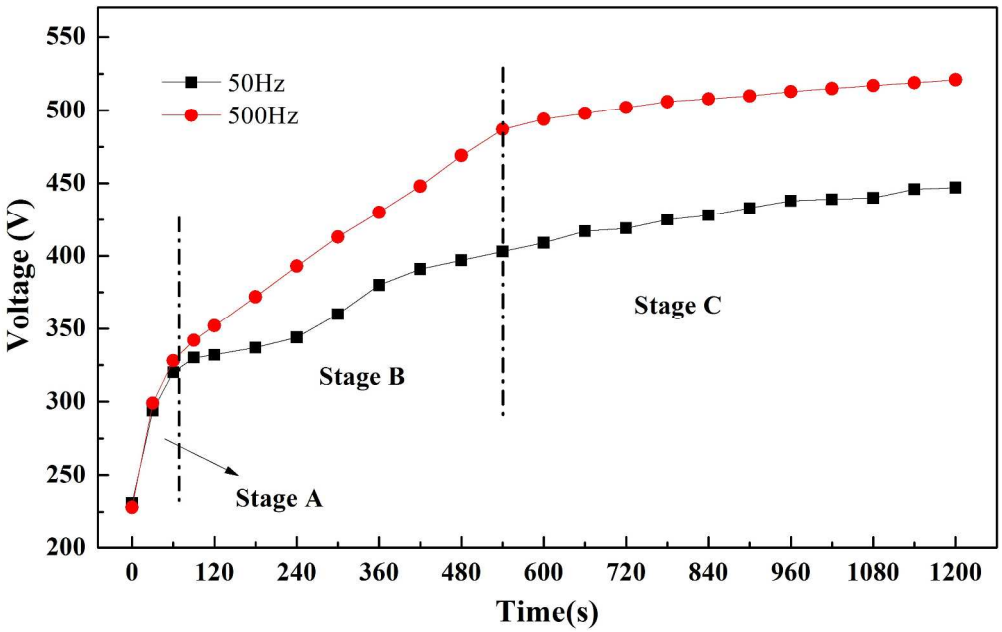

Fig. 1 Voltage–time responses during PEO processing of Mg-Li alloy at 50 Hz and 500 Hz
270x168mm (300 x 300 DPI)

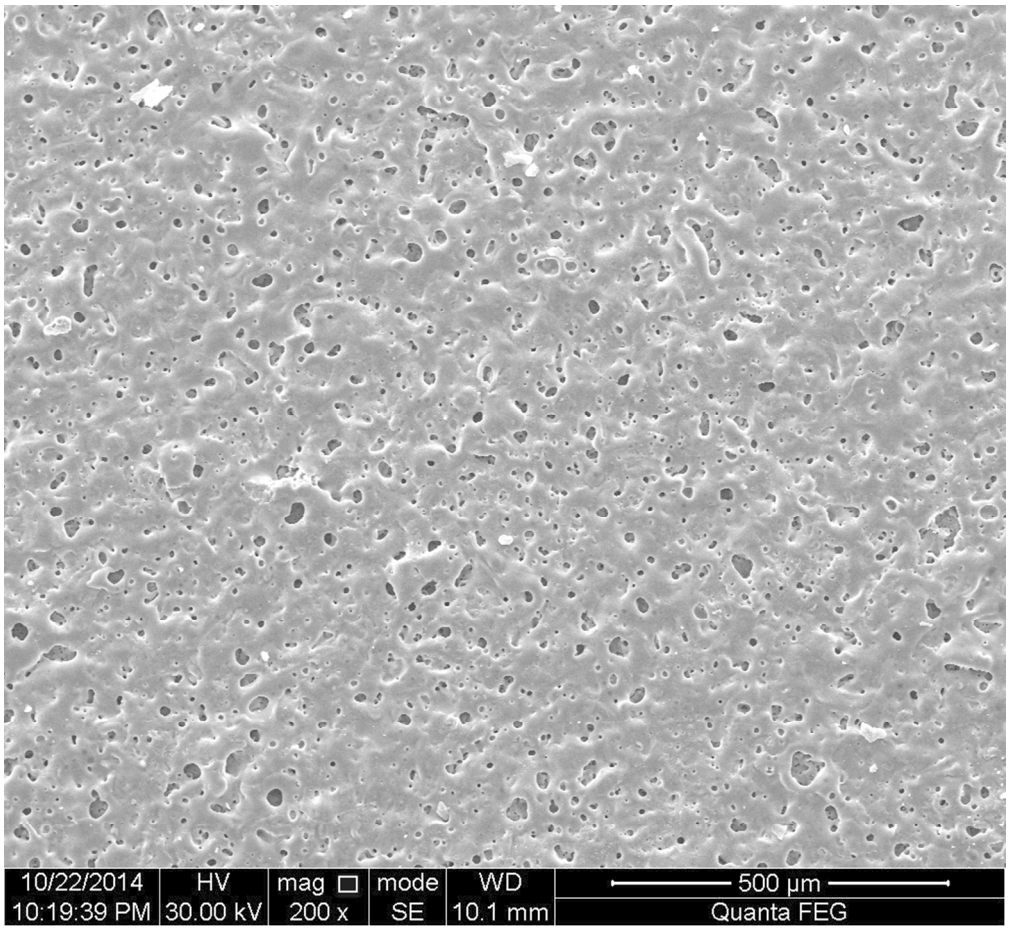

Fig. 2a The surface morphologies of the coatings prepared at (a) 300 s, 50 Hz; (b) 1200 s, 50 Hz; (c) 300 s, 500 Hz; (d) 1200 s, 500 Hz
302x278mm (86 x 86 DPI)

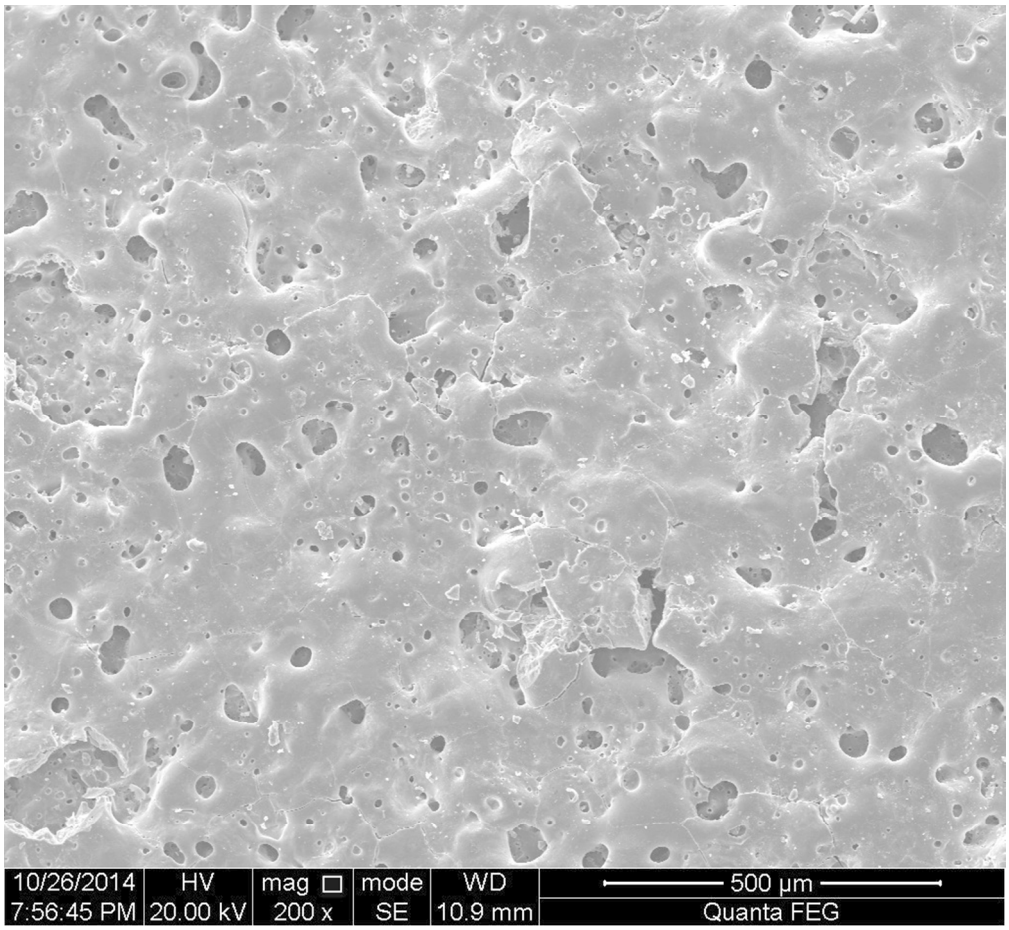

Fig. 2b The surface morphologies of the coatings prepared at (a) 300 s, 50 Hz; (b) 1200 s, 50 Hz; (c) 300 s, 500 Hz; (d) 1200 s, 500 Hz
302x278mm (86 x 86 DPI)

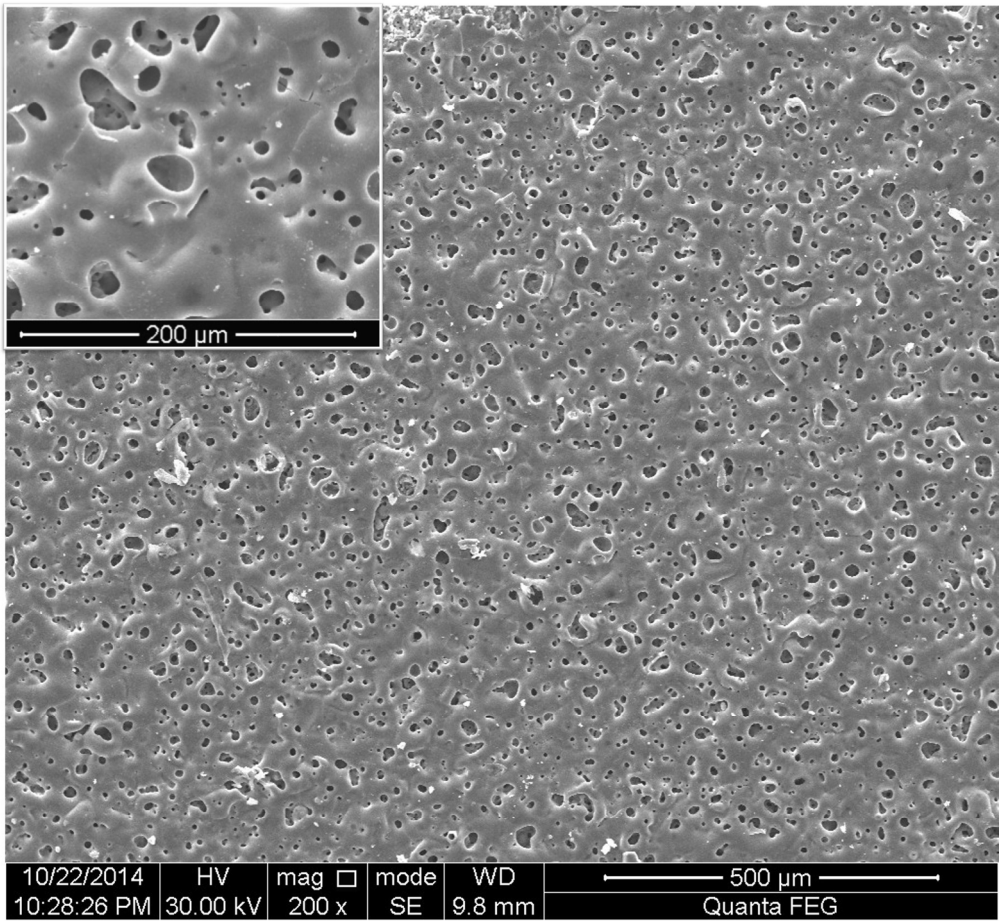

Fig. 2c The surface morphologies of the coatings prepared at (a) 300 s, 50 Hz; (b) 1200 s, 50 Hz; (c) 300 s, 500 Hz; (d) 1200 s, 500 Hz
304x280mm (150 x 150 DPI)

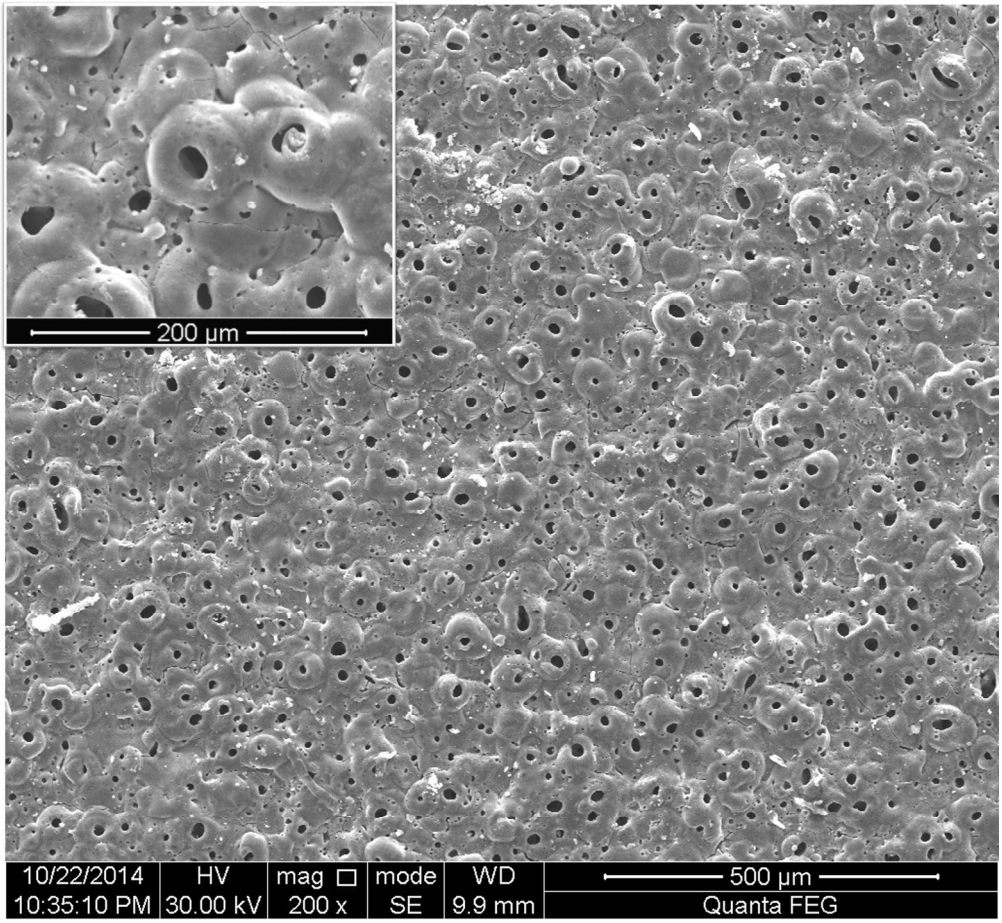

Fig. 2d The surface morphologies of the coatings prepared at (a) 300 s, 50 Hz; (b) 1200 s, 50 Hz; (c) 300 s, 500 Hz; (d) 1200 s, 500 Hz
304x280mm (150 x 150 DPI)

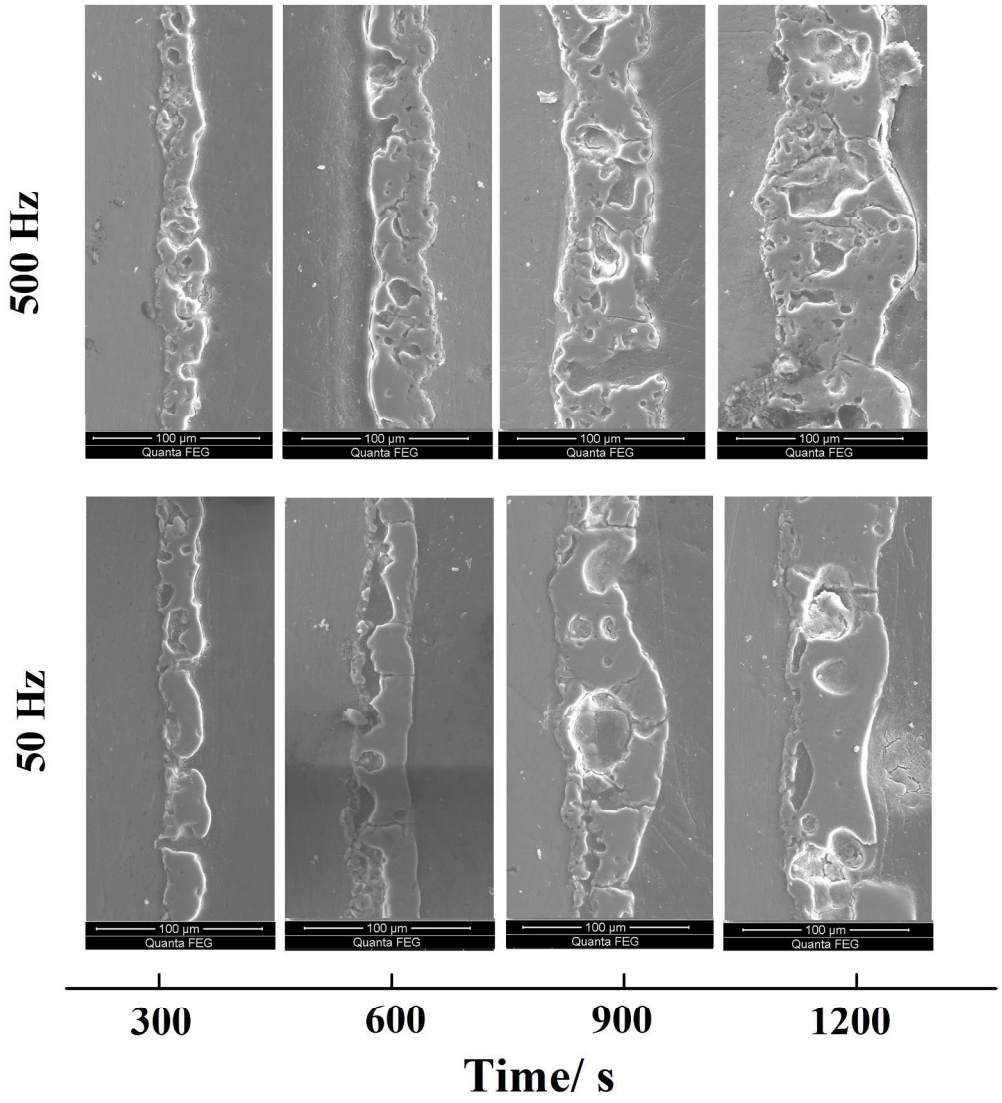

Fig. 3 Cross-sectional SEM images of the ceramic coatings
641x760mm (96 x 96 DPI)

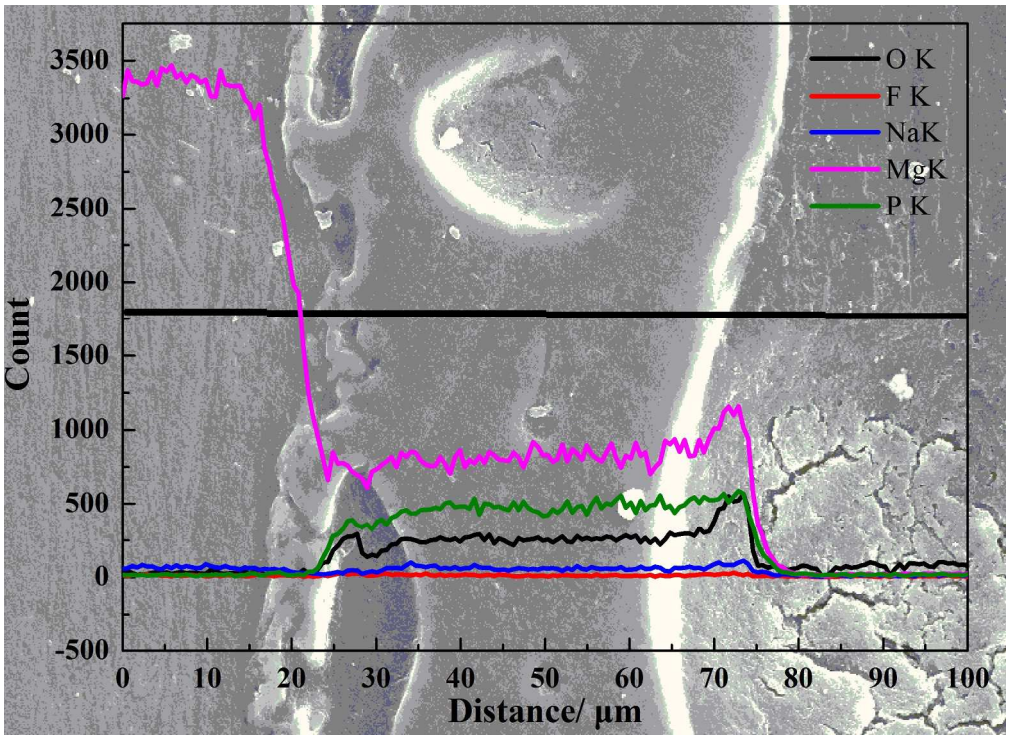

Fig. 4a The relative content of element distribution on the cross section of the PEO coatings prepared at (a) 50 Hz and (b) 500 Hz
750x546mm (96 x 96 DPI)

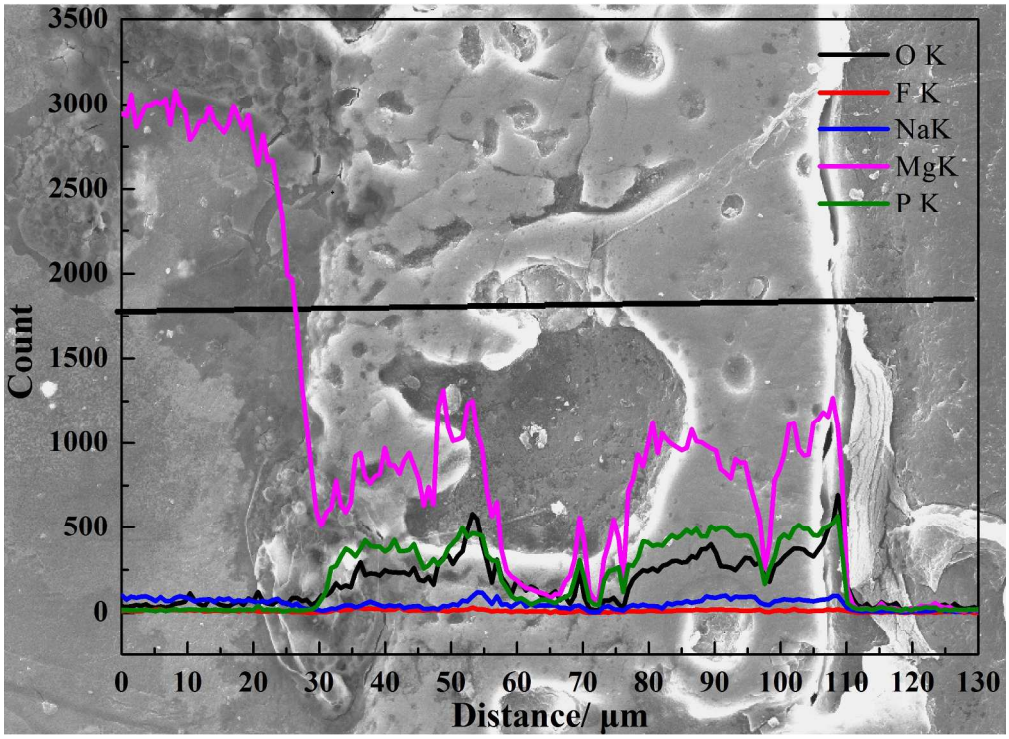

Fig. 4b The relative content of element distribution on the cross section of the PEO coatings prepared at (a) 50 Hz and (b) 500 Hz
740x541mm (96 x 96 DPI)

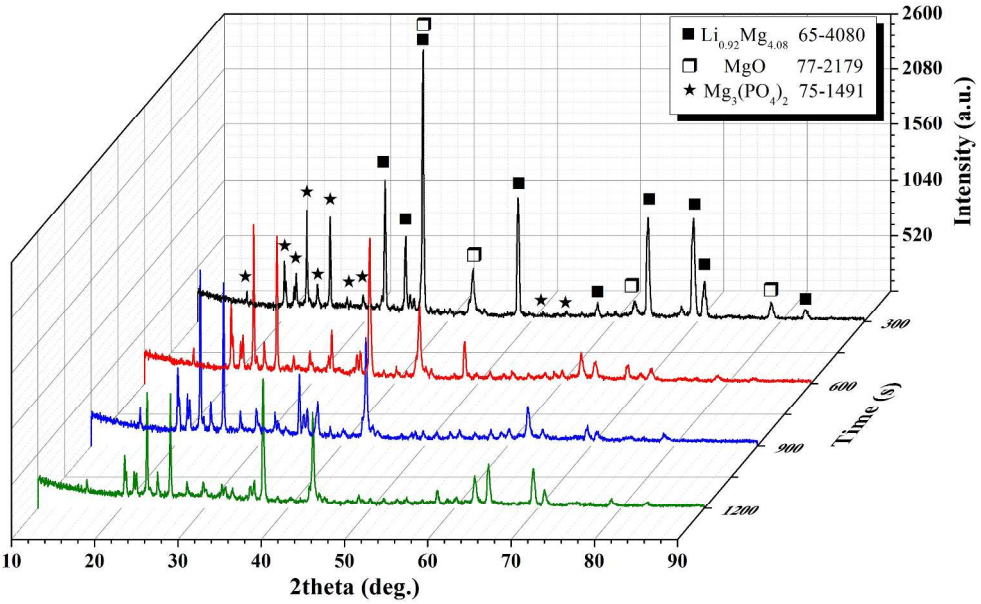

Fig. 5a XRD patterns of the ceramic coating prepared at different times, and the PEO frequency are (a) 50 Hz and (b) 500 Hz
294x199mm (300 x 300 DPI)

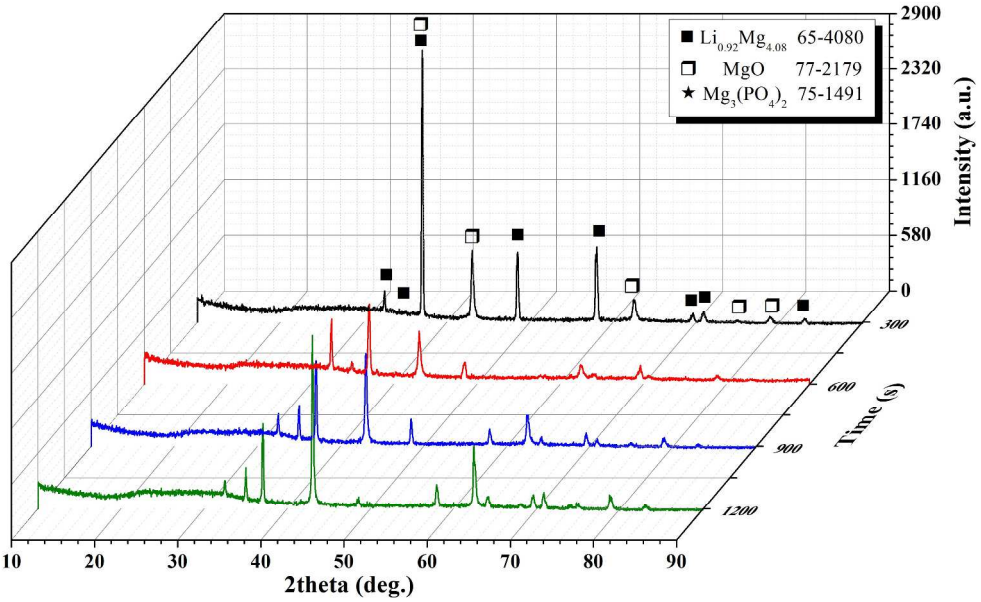

Fig. 5b XRD patterns of the ceramic coating prepared at different times, and the PEO frequency are (a) 50 Hz and (b) 500 Hz
295x198mm (300 x 300 DPI)

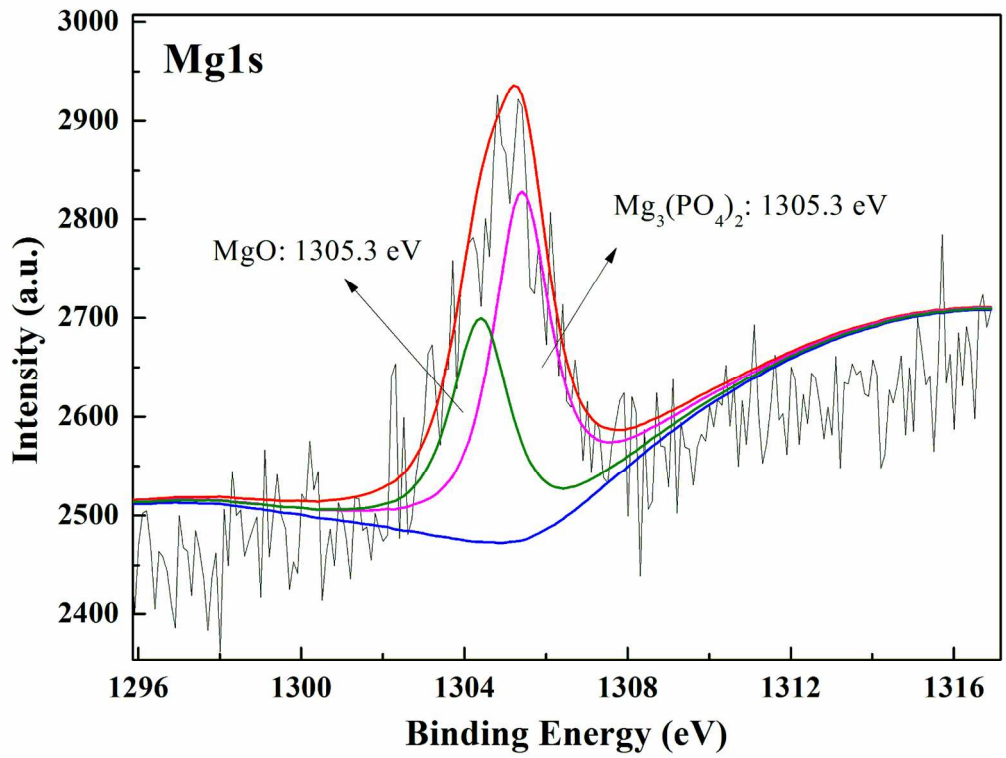

Fig. 6a The high-resolution spectra of major elements in the PEO coatings. (a) Mg 2p, 50 Hz; (b) Mg 2p, 500 Hz; (c) P 2p, 50 Hz; (d) P 2p, 500 Hz; (e) O ls, 50 Hz; (f) O 1s, 500 Hz
143x108mm (300 x 300 DPI)

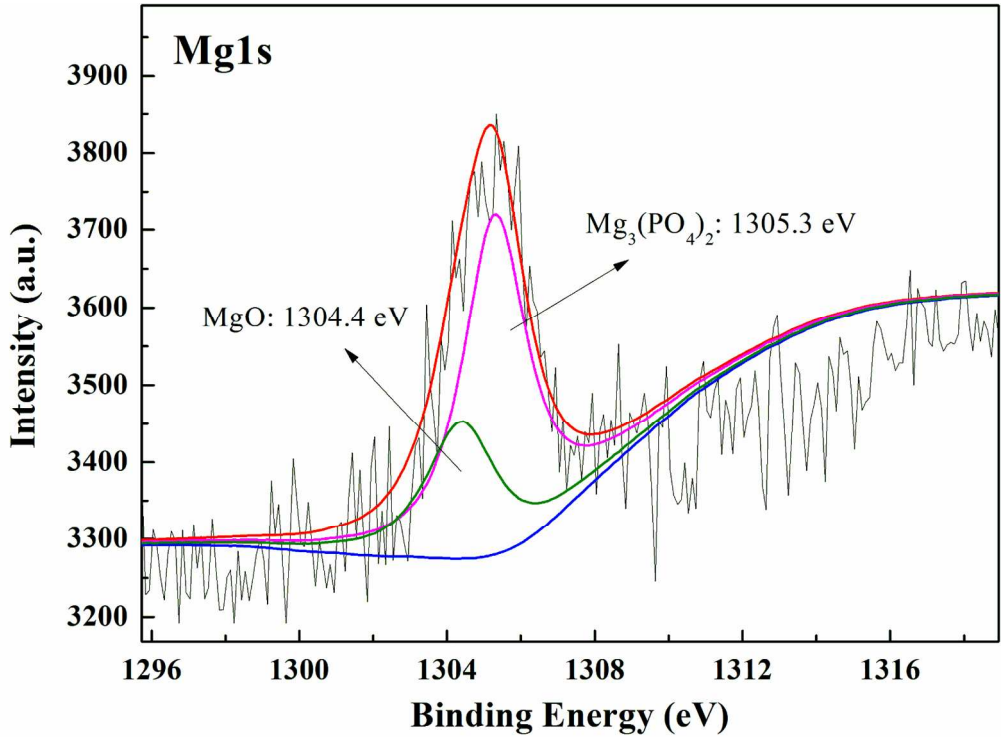

Fig. 6b The high-resolution spectra of major elements in the PEO coatings. (a) Mg 2p, 50 Hz; (b) Mg 2p, 500 Hz; (c) P 2p, 50 Hz; (d) P 2p, 500 Hz; (e) O ls, 50 Hz; (f) O 1s, 500 Hz
143x105mm (300 x 300 DPI)

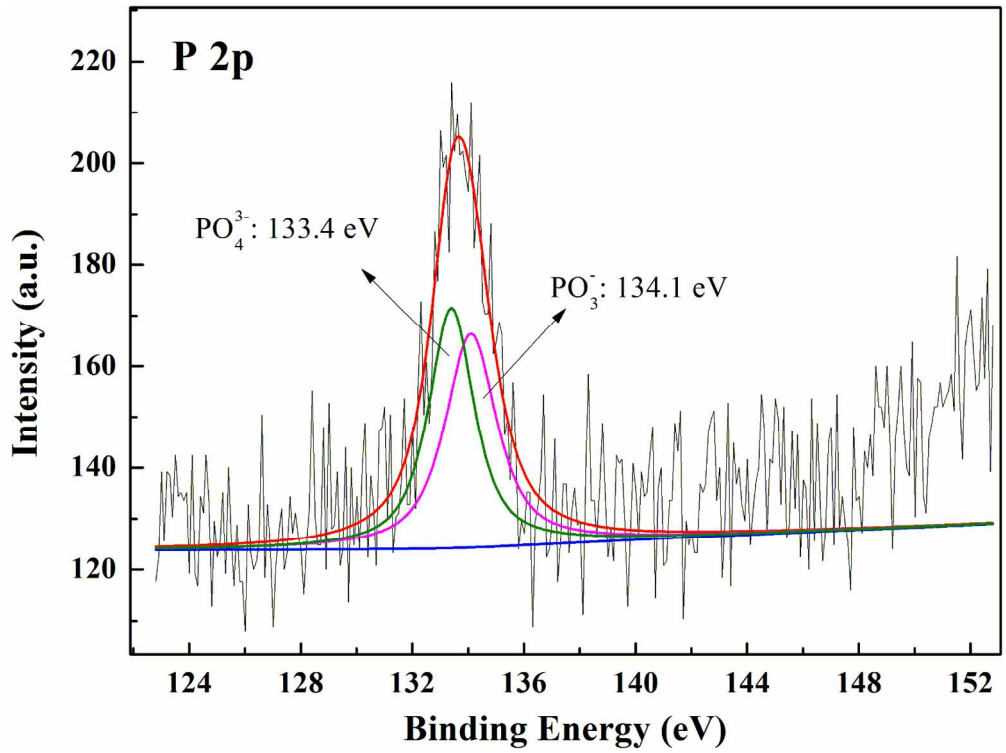

Fig. 6c The high-resolution spectra of major elements in the PEO coatings. (a) Mg 2p, 50 Hz; (b) Mg 2p, 500 Hz; (c) P 2p, 50 Hz; (d) P 2p, 500 Hz; (e) O ls, 50 Hz; (f) O 1s, 500 Hz
143x107mm (300 x 300 DPI)

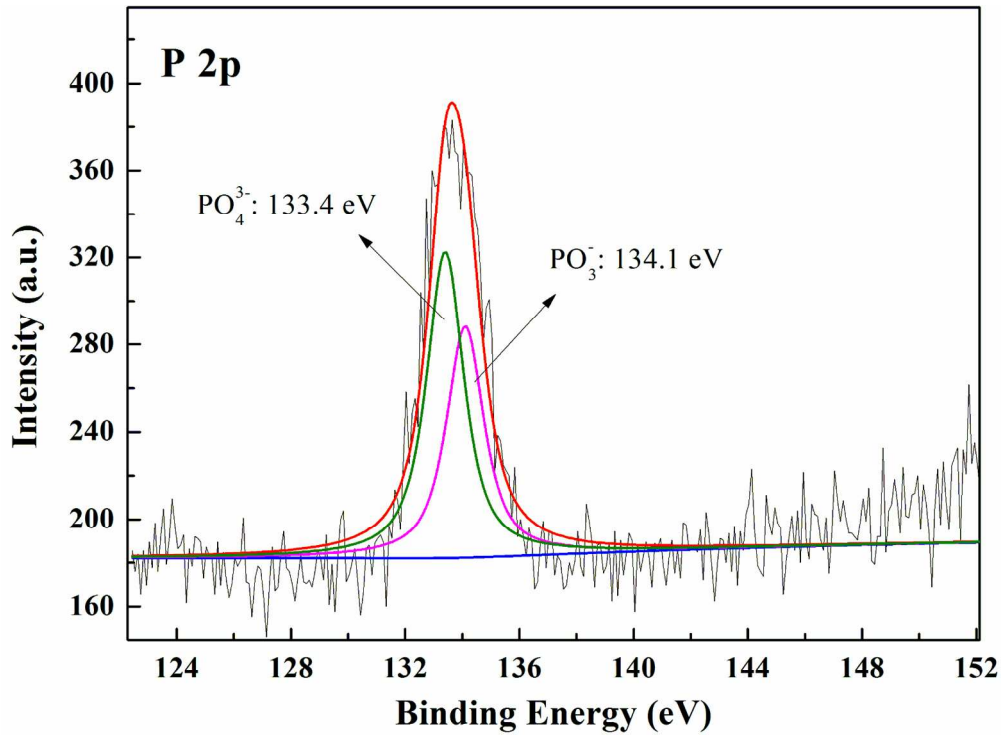

Fig. 6d The high-resolution spectra of major elements in the PEO coatings. (a) Mg 2p, 50 Hz; (b) Mg 2p, 500 Hz; (c) P 2p, 50 Hz; (d) P 2p, 500 Hz; (e) O ls, 50 Hz; (f) O 1s, 500 Hz
143x104mm (300 x 300 DPI)

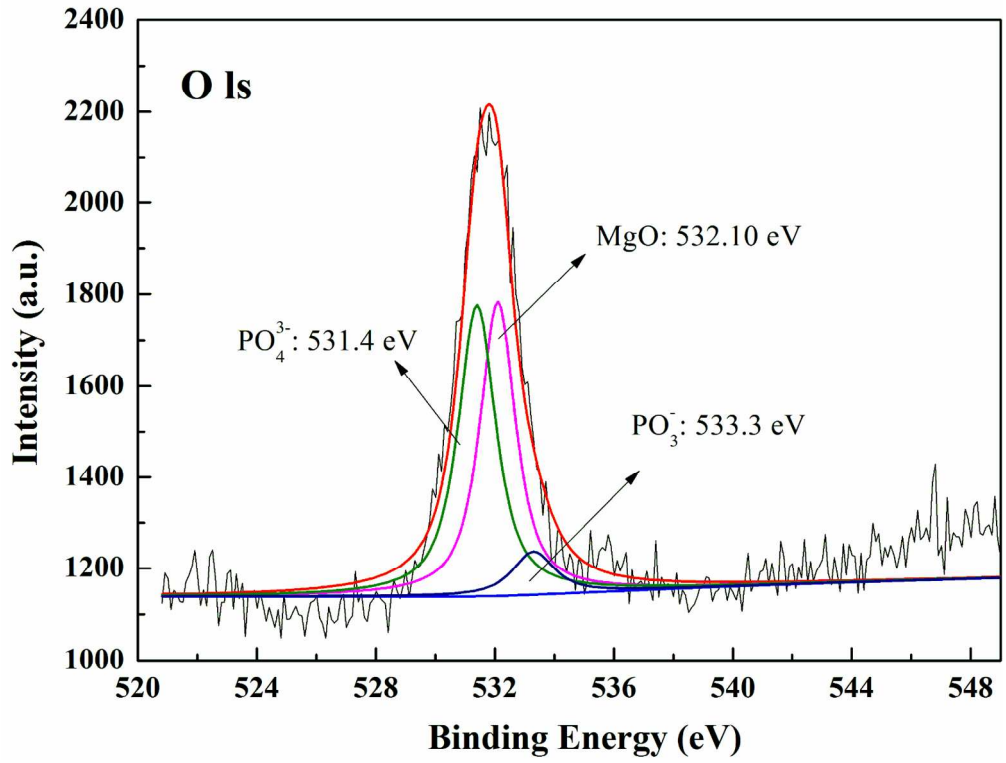

Fig. 6e The high-resolution spectra of major elements in the PEO coatings. (a) Mg 2p, 50 Hz; (b) Mg 2p, 500 Hz; (c) P 2p, 50 Hz; (d) P 2p, 500 Hz; (e) O ls, 50 Hz; (f) O 1s, 500 Hz
143x109mm (300 x 300 DPI)

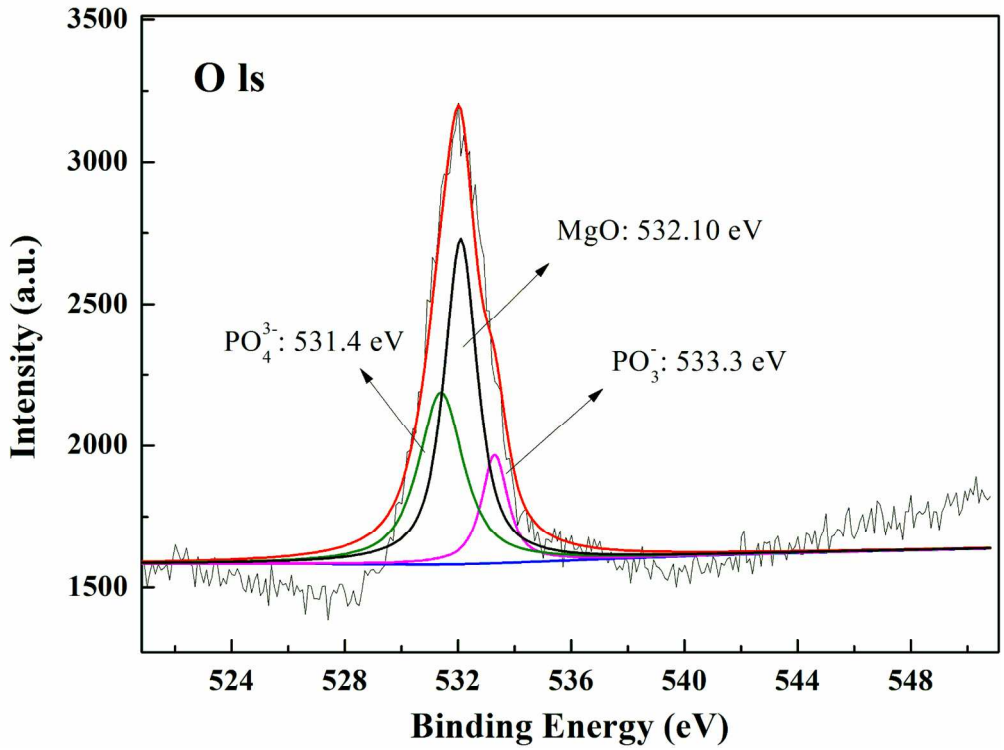

Fig. 6f The high-resolution spectra of major elements in the PEO coatings. (a) Mg 2p, 50 Hz; (b) Mg 2p, 500 Hz; (c) P 2p, 50 Hz; (d) P 2p, 500 Hz; (e) O ls, 50 Hz; (f) O 1s, 500 Hz
143x107mm (300 x 300 DPI)

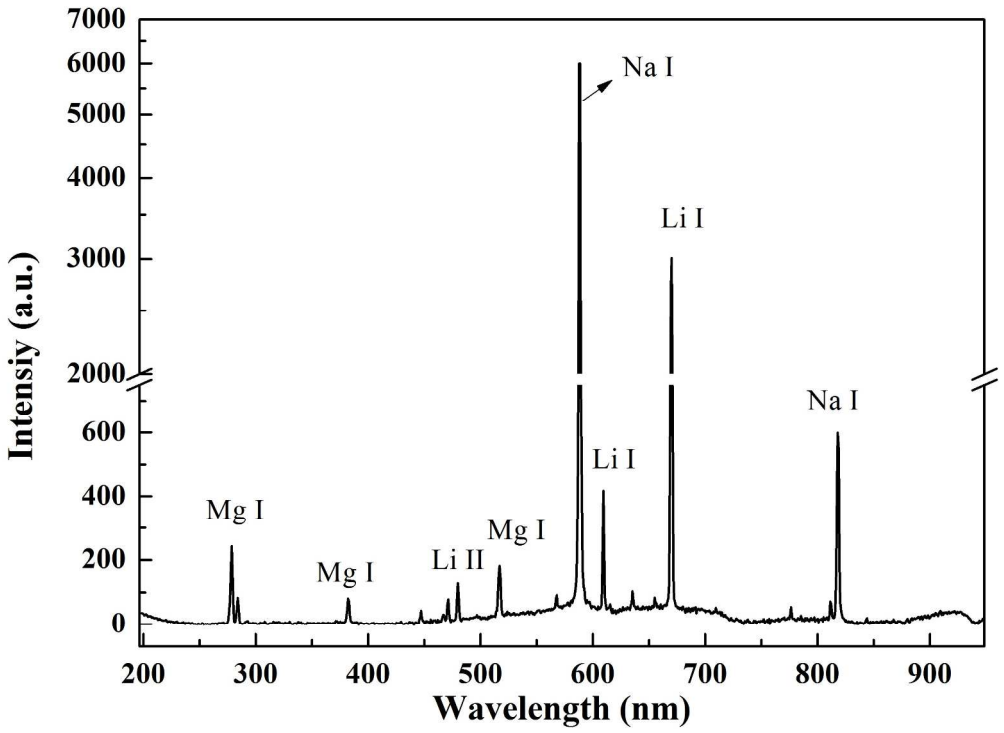

Fig. 7a Plasma Spectroscopy of PEO process at (a) 50 Hz and (b) 500 Hz for 900 s and typical time variation of the emission line intensity during the PEO process at 50 Hz (c) and 500 Hz (d)
240x176mm (300 x 300 DPI)

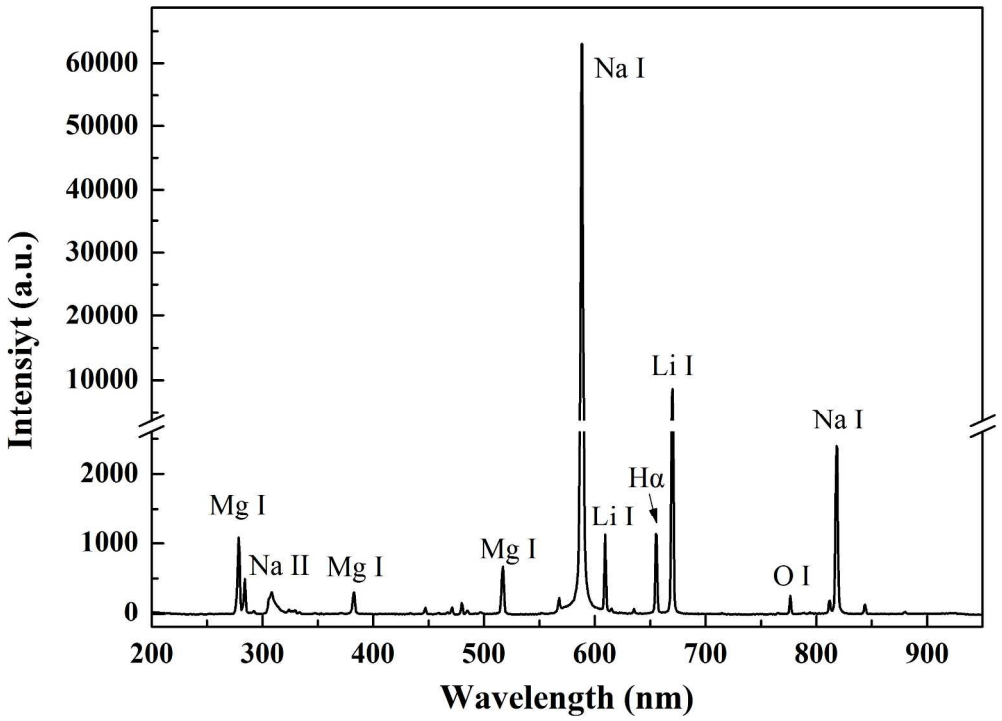

Fig. 7b Plasma Spectroscopy of PEO process at (a) 50 Hz and (b) 500 Hz for 900 s and typical time variation of the emission line intensity during the PEO process at 50 Hz (c) and 500 Hz (d)
243x173mm (300 x 300 DPI)

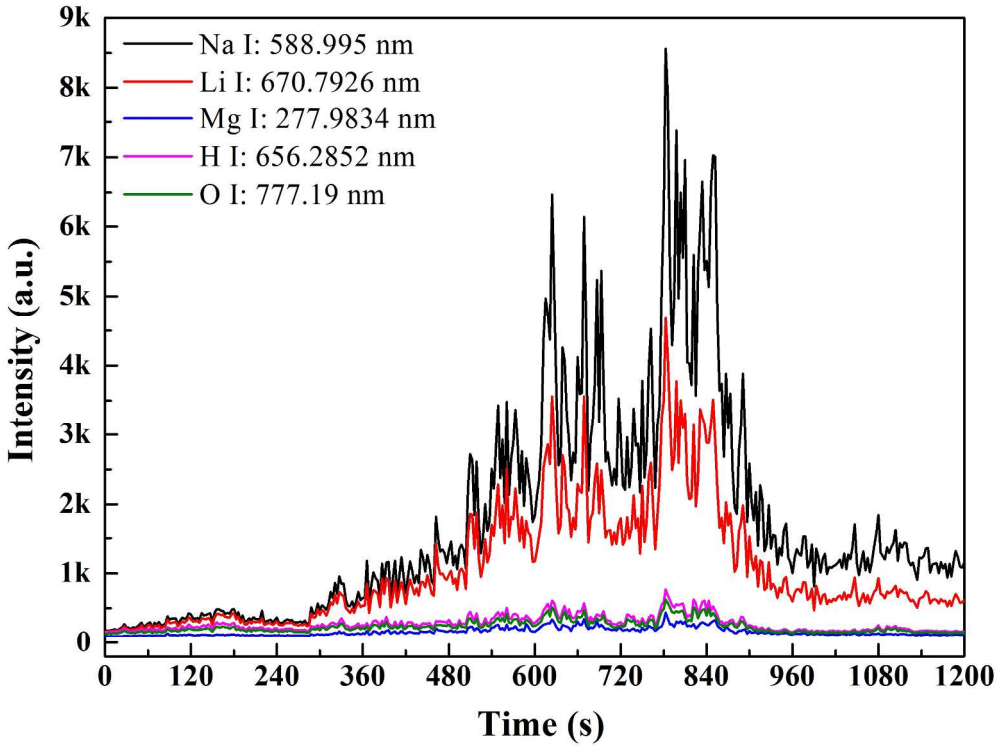

Fig. 7c Plasma Spectroscopy of PEO process at (a) 50 Hz and (b) 500 Hz for 900 s and typical time variation of the emission line intensity during the PEO process at 50 Hz (c) and 500 Hz (d)
235x176mm (300 x 300 DPI)

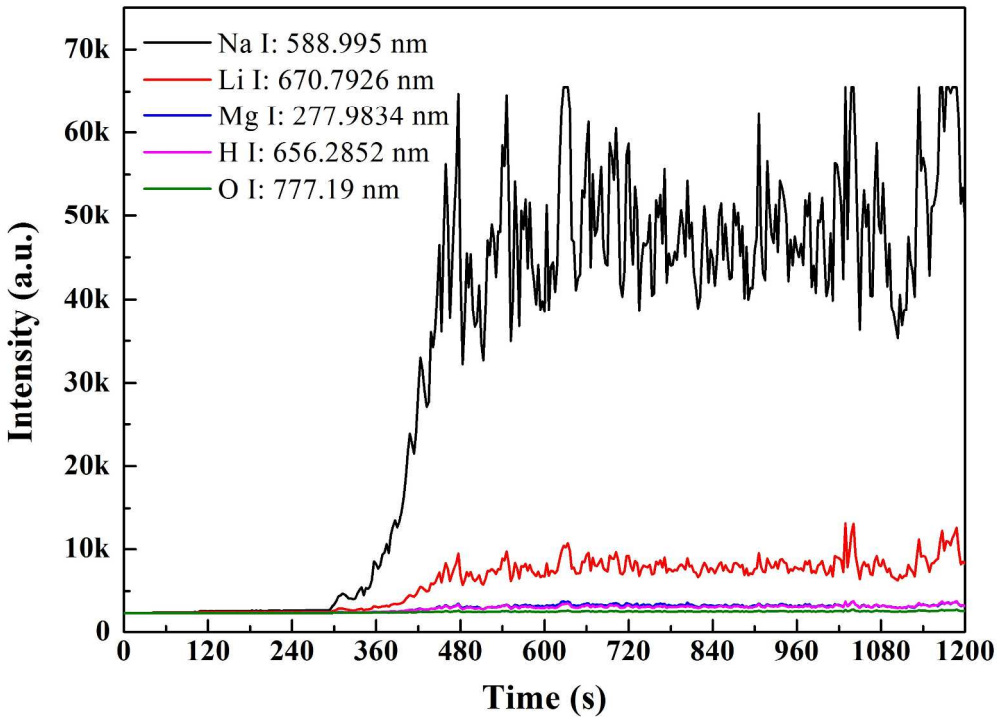

Fig. 7d Plasma Spectroscopy of PEO process at (a) 50 Hz and (b) 500 Hz for 900 s and typical time variation of the emission line intensity during the PEO process at 50 Hz (c) and 500 Hz (d)
241x171mm (300 x 300 DPI)

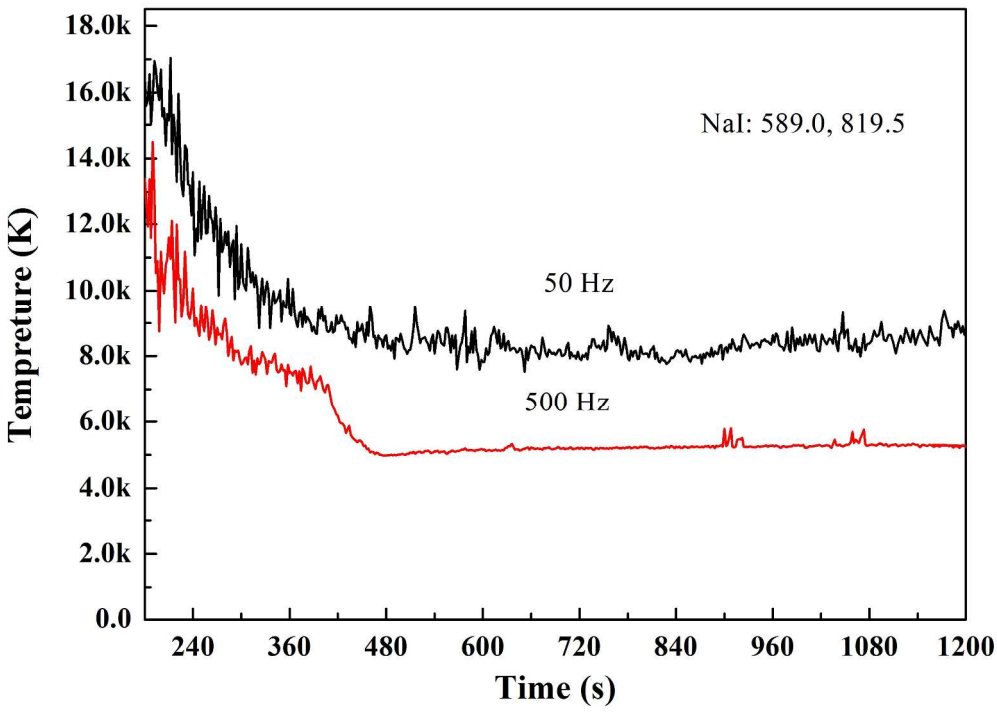

Fig. 8a Typical time variation of Te by Na I lines (a) and Na 589.0 nm / Li 670.8 nm ratios (b) at 50 Hz and 500 Hz
246x173mm (300 x 300 DPI)

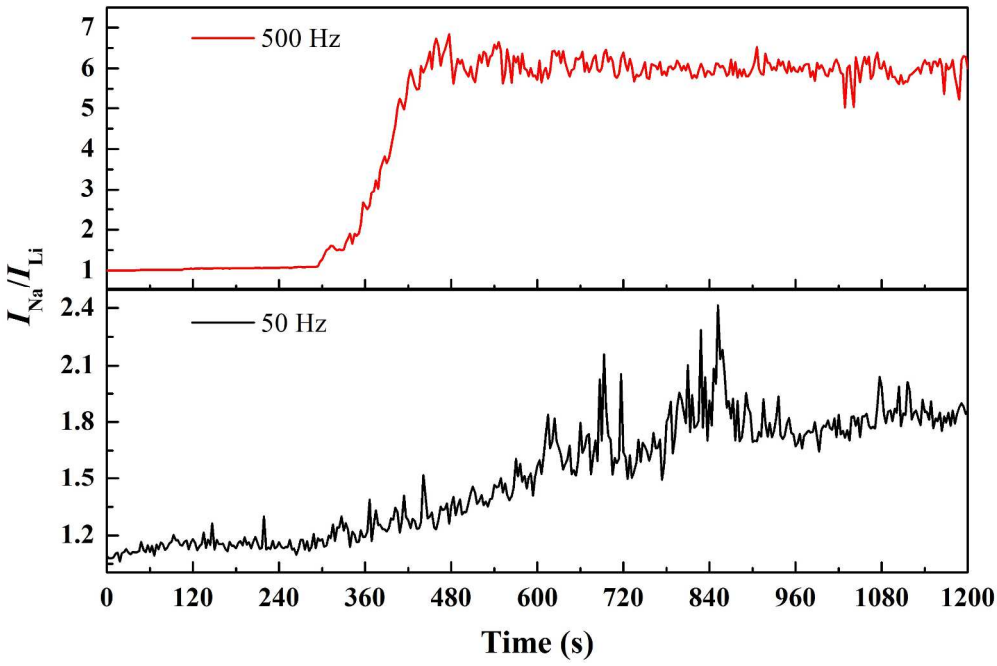

Fig. 8b Typical time variation of Te by Na I lines (a) and Na 589.0 nm / Li 670.8 nm ratios (b) at 50 Hz and 500 Hz
259x170mm (300 x 300 DPI)

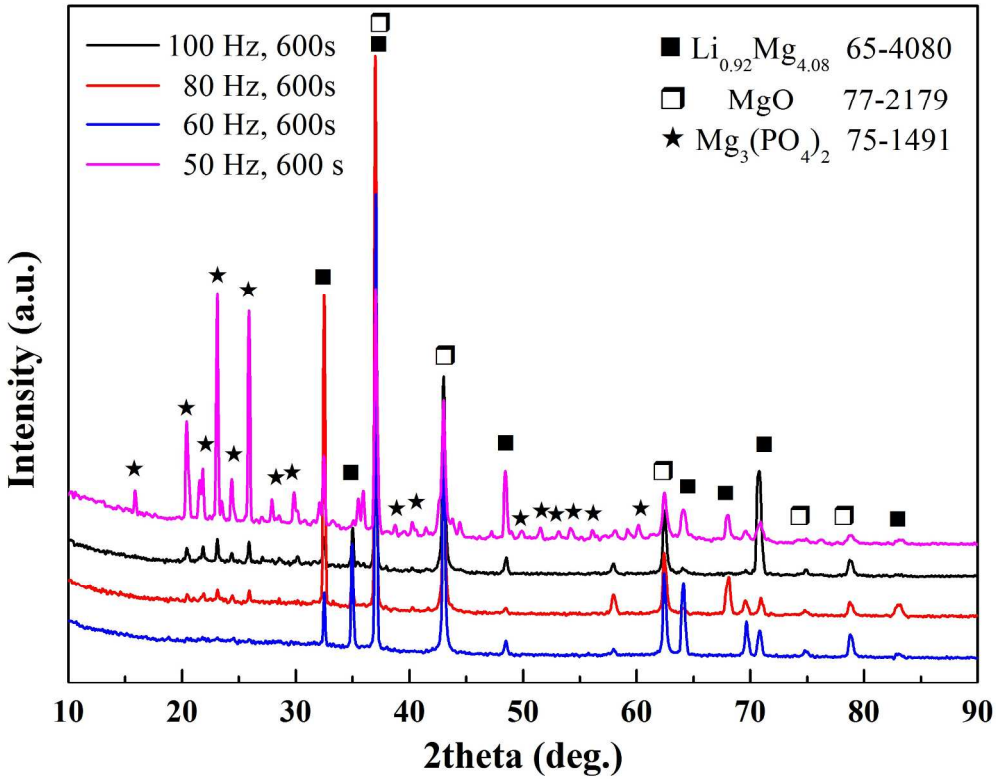

Fig. 9a XRD patterns of the PEO coating prepared (a) at different frequencies in duty ratio 20%, 5 A/dm2 and (b) in different current density and duty ratio at 80 Hz
223x172mm (300 x 300 DPI)

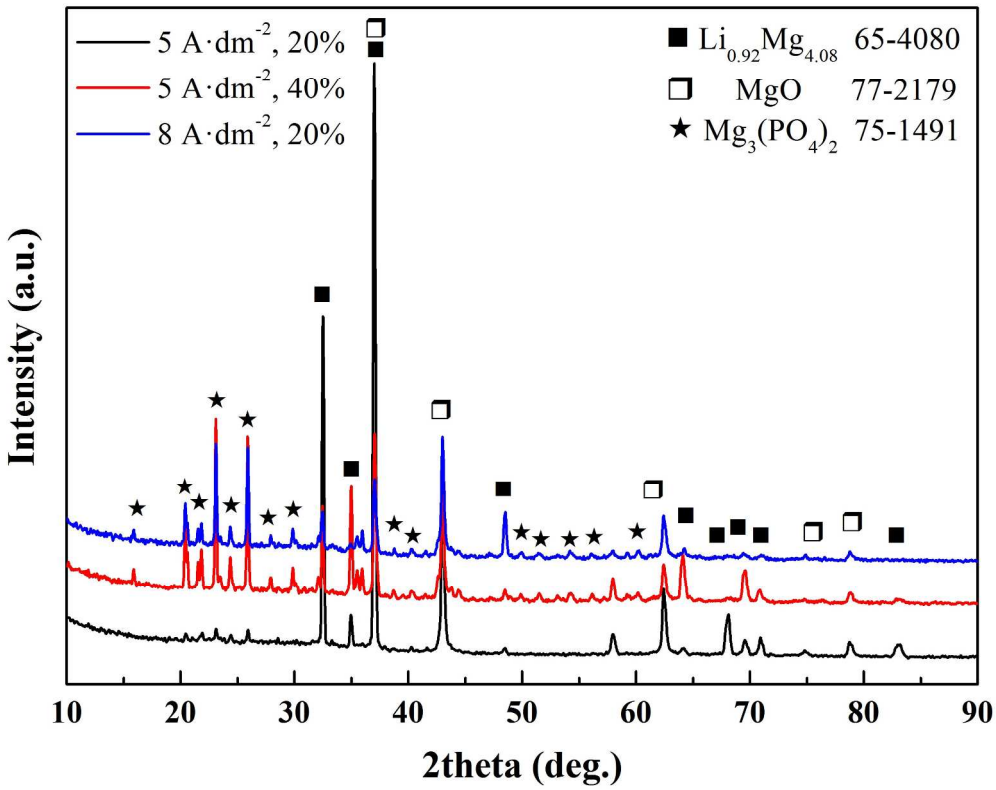

Fig. 9b XRD patterns of the PEO coating prepared (a) at different frequencies in duty ratio 20%, 5 A/dm2 and (b) in different current density and duty ratio at 80 Hz
222x180mm (300 x 300 DPI)

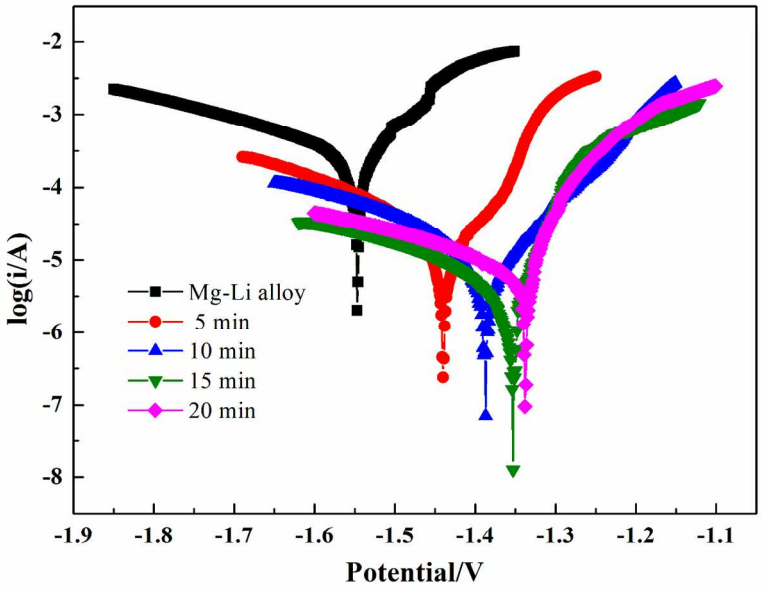

Fig. 10a Tafel polarization curves of the MAO coatings and Mg-Li alloy substrate. (a) 50 Hz and (b) 500 Hz
143x101mm (300 x 300 DPI)

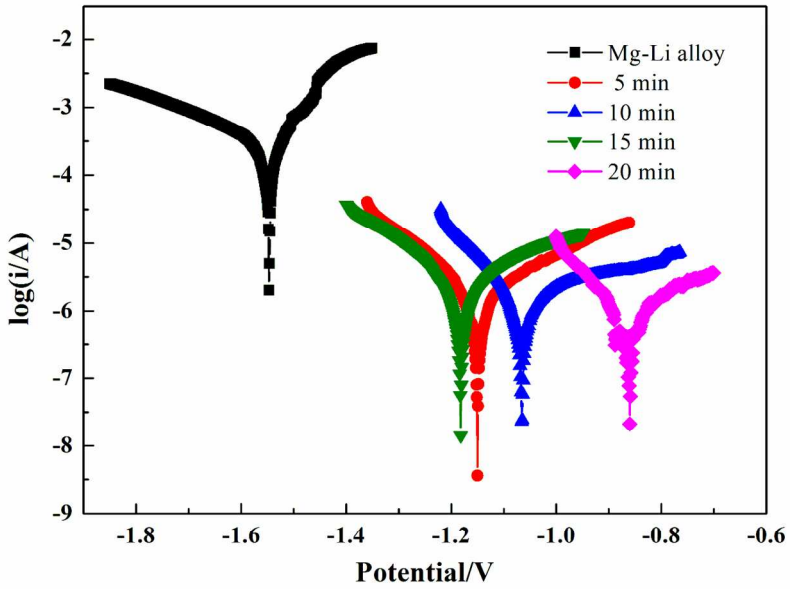

Fig. 10b Tafel polarization curves of the MAO coatings and Mg-Li alloy substrate. (a) 50 Hz and (b) 500 Hz
143x101mm (300 x 300 DPI)